Molecular Underpinnings of the Mechanical Reinforcement in Polymer Nanocomposites

Suchira Sen,[†] James D. Thomin,[†] Sanat K. Kumar,[†,§] and Pawel Keblinski*[,‡]

Isermann Department of Chemical and Biological Engineering and Department of Materials Science and Engineering, Rensselaer Polytechnic Institute, Troy, New York 12180

Received March 1, 2007

ABSTRACT: Equilibrium molecular dynamics simulations on amorphous polymers filled with solid nanoparticles show that mechanical reinforcement results from the formation of a long-lived transient polymer−particle network only over a narrow range of parameter space. In these cases it is necessary that (i) the interfacial zone occupy significantly less volume than the bulk region and (ii) particle−polymer interactions must be strong enough that the relaxation time for the small fraction of adsorbed monomers is much longer than that characterizing the neat polymer. In all other cases, reinforcement will appear to be particle driven since there is no clear demarcation between the adsorbed segments and the bulk polymer. However, the apparent size of the particle will be larger because of the adsorbed segments. Both reinforcement mechanisms occur for systems that do not easily equilibrate, leading us to stress the importance of starting states and processing history which is reminiscent of glassy systems.

1. Introduction

Experimental investigations on the mechanical properties of polymer nanocomposites have shown them to be capable of significantly more reinforcement than traditional composites.[1−3] Probably the most important experimental observation in this context is that a nanocomposite shows the appearance of a low-frequency plateau in a plot of the storage modulus vs frequency, even for spherical filler contents as small as 1%.[4−6] Similar results have also been found for platelet fillers, e.g., clays.[7−9] This plateau exists for times longer than the terminal region of the neat polymer, suggesting that its origin must be attributed to a new physical driving force. Affiliated with this result is the fact that these materials shear thin at unusually low frequencies and that their recovery to the quiescent state is very slow.[10,11] It is currently believed that these complexities arise from some combination of the following: (i) Zhu and Sternstein[12] suggest that the addition of particles to a polymer gives rise to trapped entanglements because of favorable polymer−particle interactions, which can then slow down chain dynamics. (ii) Recent work by Wang and co-workers[13] have suggested that the dominant mode of reinforcement arises from particle agglomeration, or at least from a highly nonuniform spatial distribution of particles, with polymer network formation playing a minor role.

A reasonable consequence of these statements is that the properties of these materials are controlled by nonequilibrium effects.[11,13,14] However, there really are two different schools of thought for the molecular origins of mechanical reinforcement: one is based almost exclusively on particle agglomeration, while the other attributes the findings primarily to the formation of a transient polymer network.[15] Understanding this unresolved issue is the focus of this paper.

A large fraction of simulation studies of polymer nanocomposites deal with the conformation of chains in the presence of the particles and the mobility of both species.[14,16−23] Another aspect that has been covered is particle clustering and the factors which affect it.[24,25] Only a few simulation studies[14,26−28] have directly addressed the viscoelastic properties of these nanomaterials. The work of Ganesan and co-workers,[26] which builds on the simulations of Starr and co-workers[24] and Smith et al.,[28] demonstrates that reinforcement occurs due to particle jamming at high particle loadings. Previously,[15] we utilized Monte Carlo simulations on polymer/platelet nanocomposites, which allowed us to speculate that strong polymer−particle interactions result in the formation of a solidlike network, with almost infinite relaxation times. Similarly, Ganesan and co-workers[26] provide theoretical arguments suggesting that the polymer−particle reinforcing network is important in mechanical reinforcement at low particle volume fractions. Thus, while it appears that a polymer network should play an important role in reinforcement, this has not been observed in dynamic simulations.

The objective of this work is to further explore the regions of parameter space where these different reinforcement mechanisms are important in polymer nanocomposites. Specifically, we want to find out in explicit simulations if it is possible for a particle network to be formed by the immobilization of polymer chains on particles and to investigate if such a network is capable of providing the reinforcement that has been observed experimentally.

The layout of this paper is as follows. We first discuss the static properties of the nanocomposites, specifically focusing on the dispersion of particles in the polymer matrices. Next, we will address the stress relaxation behavior. This is followed by a discussion and conclusions which will specifically address the consequences of our results on experimental findings in this area.

2. Simulation Model and Methods

2.1. Models. *2.1.1. Polymer Model.* Polymer chains are represented by the standard bead−spring Kremer−Grest model.[29] Bonded neighbors on a chain interact via a stiff FENE (finite extensible nonlinear elastic) potential: $V_{FENE} = -k(R_0^2/2)\ln(1 - (r/R_0)^2)$, where $k = 30\epsilon/\sigma^2$ and $R_0 = 1.5\sigma$. In addition, the interaction between any pair of chain monomers is purely repulsive and is described by a Lennard-Jones (LJ) potential $U(r) = 4\epsilon[(\sigma/r)^{12} - (\sigma/r)^6]$ truncated at its minimum, $r = 2^{1/6}\sigma$, and shifted so that both the potential and force go to zero at the

[†] Isermann Department of Chemical and Biological Engineering.
[‡] Department of Materials Science and Engineering.
[§] Current address: Department of Chemical Engineering, Columbia University, New York, NY.

10.1021/ma070512z CCC: $37.00
Published on Web 04/27/2007

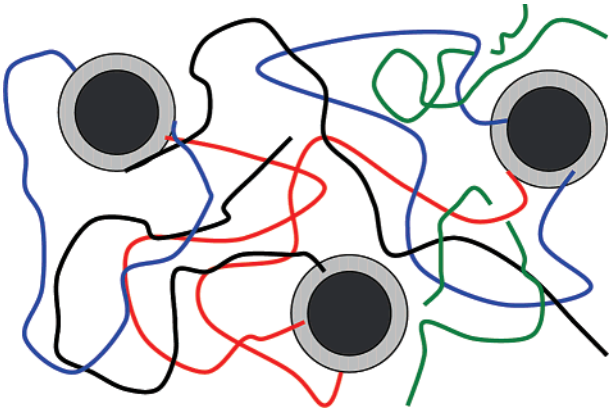

Figure 1. A schematic representation of a polymer nanocomposite (PNC). The PNC constituents are the following: black balls (fillers), gray annulus (interaction zone), green chains (free chains), red chains (bridges), blue chains (loops), and black chains (dangles).

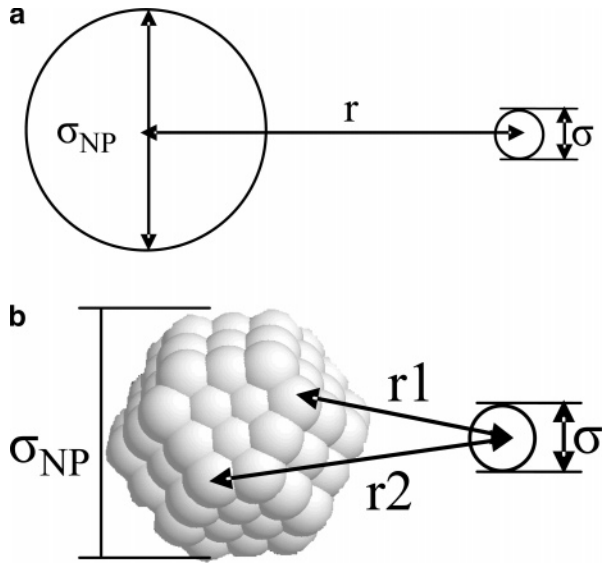

Figure 2. (a) Schematic representation of the interactions between a chain monomer and a smooth nanoparticle. (b) Schematic representation of the interactions between a chain monomer and a rough nanoparticle.

cutoff.[30,31] (All distances will be reported in reduced units, i.e., in units of σ the monomer diameter.) We model monodisperse melts of chains with degree of polymerization (N) equal to either 20 or 80. Melts of $N = 80$ chains[32] are in the crossover regime, between reptation behavior and Rouse dynamics. The $N = 20$ results, which correspond purely to Rouse behavior, allow us to make contact with the previous work of Starr et al.[24] and Smith.[28]

2.1.2. Particle Models. We have used two different particle representations: smooth (Figure 2a) and rough (Figure 2b). Reports in the experimental literature suggest that optimum property enhancements result when the size of the particle and the interparticle spacing are comparable to the size of the polymer.[6,13] Since the majority of our work focuses on chains with length $N = 80$ (RMS radius of gyration of ~4.7), we chose a particle diameter of $\sigma_{NP} = 5$.

The interactions between polymer segments and smooth particles are described in previous work.[20] The particles interact with each other through an LJ potential truncated at the minimum ($r = 2^{1/6}\sigma_{NP}$) and shifted so that it is repulsive everywhere: both the potential and the force go smoothly to zero at the cutoff.[30] A rough particle[33] is an almost spherical cluster of monomer-sized beads held together by FENE springs. To create these particles, a sphere of diameter 5 is carved out of a fcc crystal lattice of beads and the nearest neighbors connected with FENE springs which are identical to those used in the polymer chains. This results in particles that are modeled in the same spirit as those of Starr et al. and Smith et al.[22−24,28,34] Interactions between particle monomers are given by the same truncated and shifted LJ potential that was used for the polymer monomers: the same repulsive potential is employed for both inter- and intraparticle pairs. Polymer−particle interactions are governed by a truncated and shifted LJ potential[30] with various values of the parameter ϵ. Three values of the cutoff radius R_c were used: (a) $R_c = 2^{1/6}$, was used in the case of "purely repulsive" particle interactions; (b) $R_c = 2.5$, which is the typical value of the cutoff for LJ interactions, was used for "long-range" attractive potentials; and (c) $R_c = 1.5$ was used in cases where a short-range cutoff was desired. It is important to note that ϵ denotes the well depth for the unshifted polymer−particle potential. Since we truncate and shift the potential so that it assumes a potential and force equal to 0 at the cutoff, the effective well depth is smaller in magnitude than ϵ. While this correction is small for $R_c = 2.5$, it is much bigger for $R_c = 1.5$. Since the actual well depth gives a measure of the binding energy, we report this value as w in the text and will omit reporting ϵ.

2.2. Methods. *2.2.1. Simulation Methods.* Simulations were performed in the NVT ensemble. The temperature was kept constant at $T^* = 1$ by direct velocity rescaling.[31] The monomer number density of the melt was constant at $\rho^* \approx 0.85$ for all simulations. For the filled systems the volume of the simulation box was increased so that the volume available to the polymers was the same as for the neat systems. The velocity-Verlet[31] algorithm was used to integrate the equations of motion, with a time step $\delta t = 0.005$, where time has been reduced by τ, the Lennard-Jones time. Additional details about the methods used can be found in ref 32.

The number of nanoparticles in all cases was $N_p = 4$, which were placed initially at the fcc sites of the cubic simulation cell. Typical systems were comprised of 2400 chain monomers, and the size of the cubic simulation box was ~14. Additional systems with 4800 and 6800 monomers were also studied in a few cases. Thus, depending on system size, we employed particle loadings of volume fraction $\varphi = 0.089$, 0.045, and 0.033, respectively. The neat systems used for comparison consisted of 2400 chain monomers.

To generate the initial structures, in most cases we placed the polymer chains in a large box in a stretched, linear configuration. The system, which was thus at some arbitrarily low density, was then compressed using an NPT simulation to the proper melt density *without attractive interactions*. Once the appropriate density was reached and the chains had relaxed, the attractions were turned on. All of the simulation runs consisted of an equilibration phase followed by a production phase. In the case of weakly interacting or repulsive particles, the systems were equilibrated after a time in the range 10 000−50 000. (The relaxation time for melts of $N = 80$ chains was 30 000.) A typical production run in these cases would span a time of 200 000−2 000 000. It is important to note that, for strongly attractive particles (rough particles with short-ranged attractions), the binding energy is ~5.1, giving the surface layer an effective temperature, kT/w, of ~0.2, which is well below the glass transition temperature at this density.[35] Consequently, in these cases the systems do not truly equilibrate within accessible run times. This fact will be reiterated and discussed in detail in the results and conclusions sections.

2.2.2. Analysis Methods. The structural properties of the melt were characterized by the mean-squared radius of gyration $\langle R_g^2 \rangle$ and the mean-squared end-to-end distance $\langle R_e^2 \rangle$. We also calculated the radial pair distribution function [$g(r)$] for the centers of mass of the particles to determine particle dispersion.

System dynamics were characterized by the end-to-end vector autocorrelation function of the chains and the average mean-squared displacements (MSD) of the chains and particle centers-of-mass as a function of time. Diffusion coefficients for both particles and chains were then obtained using the Einstein equation, $g_3(t) = \langle |r_{cm}(t) - r_{cm}(0)|^2 \rangle = 6Dt$.[36]

The intent of this work is to study the viscoelastic properties of these systems. Thus, most of our discussion will focus on the stress autocorrelation function (ACF), which we will also refer to as the stress relaxation function. This quantity is computed by first calculating the off-diagonal elements of the stress tensor as defined by the atomic virial,[31] $\sigma_{\alpha\beta} = (1/V)(\sum_i p_{i\alpha}p_{i\beta}/m_i + \sum_i \sum_{j>i} r_{ij\alpha}f_{ij\beta})$, where $\alpha \neq \beta$ and indicate the *xyz* vector components, the subscripts *i* and *j* are atomic indices, *p* is the momentum, *m* is the mass, *r* is the radial separation, and *f* is the force. The stress ACF is then given by $\langle \sigma_{\alpha\beta}(t)\sigma_{\alpha\beta}(0) \rangle$, where $\langle ... \rangle$ denotes an average over time. As in our previous work,[32] we "smoothed" the ACF by using interval averages. The stress ACF was truncated once its value dropped below 10^{-4}, below which noise dominates. However, integration was performed over the full "raw data" ACF function. The stress ACF corresponds to the time-dependent stress relaxation after a step strain. A Fourier transform of this function yields the storage and loss modulus as a function of frequency. We have also calculated these quantities, but in the interest of space we show only the stress ACFs. The zero shear rate viscosity is calculated using the Green−Kubo relation:[31] $\eta = (V/T)\int_0^\infty \langle \sigma(t)\sigma(0) \rangle \, dt$.

3. Results and Discussion

3.1. Static Properties of the Melt. The rms radius of gyration $\langle R_G^2 \rangle^{0.5}$ and rms end-to-end distance $\langle R_e^2 \rangle^{0.5}$ were found to be unperturbed within the uncertainty of the calculation on the addition of nanofillers. This result is independent of the nature of the particle (smooth vs rough) or of the polymer−particle interactions. This finding is similar to many reports in the simulation literature,[18] although it remains experimentally unverified.[38,39]

3.2. Chain and Particle Dynamics. At any given time the chain mean-squared displacement (MSD) increases on the addition of repulsive particles but decreases when polymer−particle interactions are attractive (Figure 3a,b). The diffusivity also decreases with increasing volume fraction of filler. Particle motion follows a trend similar to that of the chains and is slowed down with increasing attraction and with increasing particle loadings (Figure 3c). However, the change in particle motion is much more pronounced than that of the polymers. In particular, for $w = 5.1$, the particles become strongly localized. This result might reflect the fact that each particle has multiple chains "attached" to it. Hence, its motion requires that all of the chains move in a "cooperative" fashion.[20]

3.3. Particle Clustering. The state of particle dispersion is important for several reasons. Clustering of the nanoparticles reduces the intermixing of polymer and nanoparticles, thus reducing the interfacial area. Wang et al.[13] suggest that this clustering can lead to reinforcement: if true, this conclusion has far-reaching consequences since it suggests unusual nanocomposite properties bear no relationship to the chain nature of the polymer matrix. The opposite limit is that the formation

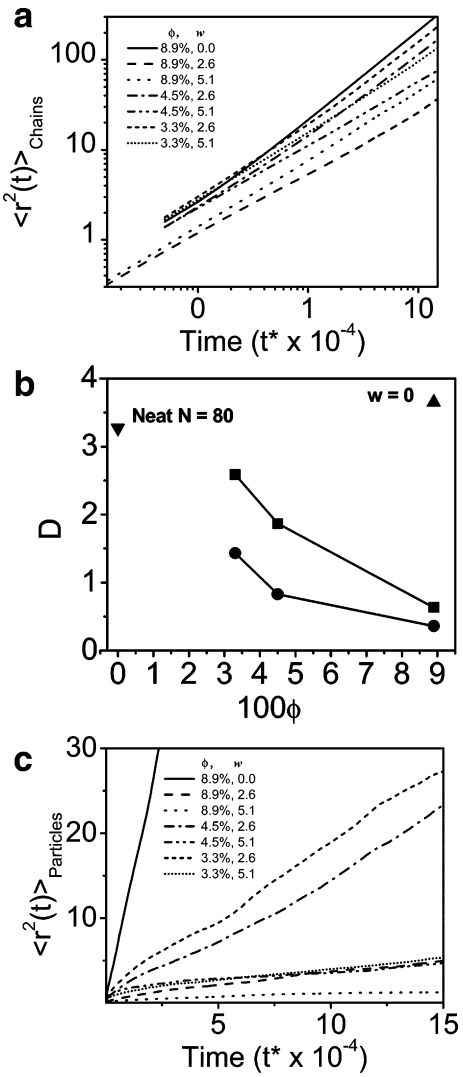

Figure 3. (a) Mean-squared displacement of chain center-of-mass compared for systems at different particle loadings and different polymer−particle interactions [ϕ, w]: [0.089, 0.0] (solid), [0.089, 2.6] (dash), [0.089, 5.1] (dot), [0.045, 2.6] (dash dot), [0.045, 5.1] (dash dot dot), [0.033, 2.6] (short dash), [0.033, 5.1] (short dot). (b) Diffusivity of chains as a function of particle loading and polymer−particle interaction. The polymer−particle interaction for the systems is LJ with short cutoff of 1.5: neat melt with $N = 80$ (inverted triangle), $w = 0$ (triangle), $w = 2.6$ (square), $w = 5.1$ (circles). (c) Mean-squared displacement of particles compared for systems at different particle loadings and different polymer−particle interactions [ϕ, w]: [0.089, 0.0] (solid), [0.089, 2.6] (dash), [0.089, 5.1] (dot), [0.045, 2.6] (dash dot), [0.045, 5.1] (dash dot dot), [0.033, 2.6] (short dash), [0.033, 5.1] (short dot). The polymer−particle interaction for the systems is LJ with short cutoff of 1.5, and we considered chains of length $N = 80$.

of a transient polymer network is critical for reinforcement. This requires that particles are well dispersed in the polymer, so that the average interparticle spacing is on the order of the polymer size. An intuitive means of improving particle dispersion is to increase the attraction between polymer segments and the filler,[24] thus making a large interfacial area energetically more favorable. To that end, we have examined systems with a range of well depths (w) equal to 0, 0.06, 2.6, and 5.1 ($R_c = 1.5$) to delineate the role of polymer−particle attractions in this respect. (For this form of the potential energy equation, when $w = 0.06$, the effective particle diameter is slightly less than it would be in a purely repulsive system.) The systems contain 30 chains of length 80, and 4 rough particles, unless otherwise noted.

Agglomeration is characterized by the particle−particle radial distribution function, $g(r)$ (Figure 4a). For $w = 0$, the repulsive

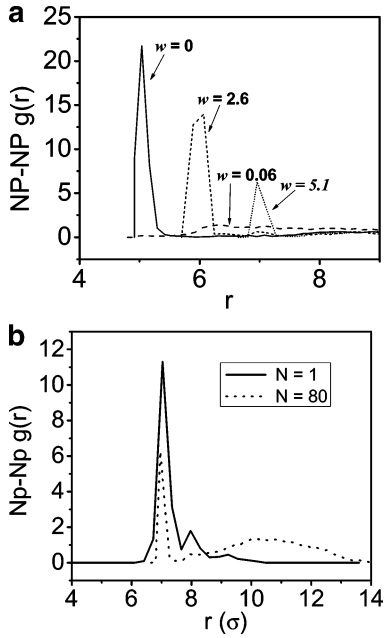

Figure 4. (a) Particle−particle radial distribution function (rdf) at varying levels of polymer−particle attraction. These data corresponded to $N = 80$ systems with rough particles, $R_c = 1.5$, and a variety of w values. The full line is for $w = 0$, the long dash for $w = 0.06$, short dash for $w = 2.6$, and dash-dot for $w = 5.1$. (b) Particle−particle rdf for a system with $N = 80$ chains and a system with $N = 1$ monomers, both at the same particle loading ($\phi = 0.089$) and $w = 5.1$, $R_c = 1.5$.

particle−polymer interaction potential, there is a strong peak in $g(r)$ at ∼5 (the particle diameter), corresponding to direct contact aggregation. This result is a consequence of polymer-induced particle−particle attractions.[40] For a weak attraction ($w = 0.06$) $g(r)$ smoothly increases from zero starting at $r = 5$ and becomes essentially equal to unity for $r > 6$, consistent with good particle dispersion. These results echo the previous findings of Starr et al.,[24] who showed that one can go from clustered to dispersed states by increasing the attraction between the polymer and particle. When the attraction is increased to $w = 2.6$, clear peaks are visible at $r = 6$ and $r = 7$. This is a signature of "bridging clustering" of nanoparticles via one or two monolayers of the polymer melt. At even higher attraction, $w = 5.1$, the peak at 6 disappears, while a single peak in the vicinity of 7 remains. We have also considered the case where $w = 5.1$, but with chain length $N = 1$ (i.e., monomers). We find that the results are similar to those found for the polymeric case (Figure 4b). Since both the chain and the monomer systems show a peak in the vicinity of 7, we argue that this must simply be a consequence of a layer of monomers that are effectively "pinned" to the particle surface. Due to the short range of the LJ interactions ($R_c = 1.5$), no additional layers of monomers are adsorbed. The bound layers effectively increase the diameter of the particles by 2, and the resulting structures undergo aggregation,[25,41] corresponding to the peak at 7. Note also that the chain molecule case in Figure 4b has an additional peak at larger distances. We attribute this peak to the formation of a polymer-mediated network. We compare these findings with the recent results of Hooper and Schweizer.[25] Using PRISM theory, these workers suggested that the dispersion state of particles in a dense polymer melt falls into four categories: (i) direct contact aggregation due to polymer-driven attraction, (ii) steric stabilization with noninterpenetrating adsorbed polymer layers, (iii) segment level tight particle bridging, and (iv) "tele-bridging" where distinct adsorbed layers coexist with longer range bridging. On the basis of this model, we suggest that the system with $w = 0$ is in category (i), $w = 0.06$ category (ii), and $w = 2.6$ category (iii). It also appears that the $w = 5.1$ system is in category (iv). It must be stressed that for $w = 5.1$ the chain segment desorption times become very long. Because of this fact, we cannot say whether these results represent the true equilibrium properties of the system.

3.4. Reinforcement. *3.4.1. Defining Stress Reinforcement.* Experiments have shown the appearance of a low-frequency plateau in the storage modulus, which persists to frequencies lower than the terminal region of the neat polymer.[4−9,13] In our simulations, the polymer chains are not long enough to exhibit a prominent entanglement plateau in the stress relaxation function. Because of this, in the neat melt we observe simple Rouse relaxation, followed directly by the exponentially decaying terminal region. To make the connection between our simulations and the reinforcement seen in experiments, we must therefore look for signs of non-Rouse-like behavior, most prominently a plateau in the stress relaxation function rather than a simple increase in viscosity due to a uniform shift in magnitude of the stress relaxation function.

3.4.2. Nonreinforced Systems. The nonreinforced systems can be broadly classed into two categories: those with repulsive interactions and those with attractive interactions.

We begin by considering the case with $w = 0$, where the polymer−particle interaction is repulsive. These simulations were performed using rough particles, since smooth particles were found to overlap significantly after forming a cluster. For particle volume fractions of 8 and 15% for both $N = 20$ and $N = 80$ we find moderate increases in viscosity. This result appears to be contrary to a number of results obtained in experiment and in simulations. Mackay and co-workers[42] have found that the viscosity of polymers filled with particles made of cross-linked, collapsed single chains with the same chemical structure as the matrix decreased rather than increased as predicted by the Einstein formula. Kairn et al.[43] have also observed viscosity decreases, in both simulations and experiments. These observations were consistent with Smith et al.'s[28] molecular simulation results for a system involving a single particle surrounded by polymer melt: they also found that viscosity decreases for repulsive interactions.

This apparent contradiction can be rationalized with a theoretical framework developed by Ganesan and co-workers.[44] Within this framework, the viscosity of the polymer melt is affected by repulsive particles in two distinct ways. The first effect is the "interfacial zone" effect and is due to the fact that the local mobility of polymer chains within $\sim R_g$ distance from the particle surface is dependent on the particle−polymer interactions. For repulsive interactions this local mobility increases relative to the pure melt (see e.g. ref 20). This mobility increase leads to a decreased viscosity. The second is the hydrodynamic effect leading to an increase in the melt viscosity due to interactions of hydrodynamic fields induced by particle motion as given, for example, by the Batchelor−Einstein formula.[3] Therefore, we speculate that, at higher volume fractions, nonlinear hydrodynamic effects dominate the system, leading to viscosities higher than that of a pure melt. To support our interpretation, we have conducted further simulations of a system with low (∼2%) particle volume fraction and indeed observed viscosity decreases.

We next move to the case of smooth attractive particles. The stress relaxation functions of a few representative systems at volume fraction $\phi = 0.089$ and with various values of w are shown in Figure 5a. All systems exhibit Rouse behavior with the main effect of adding attractive nanoparticles being a

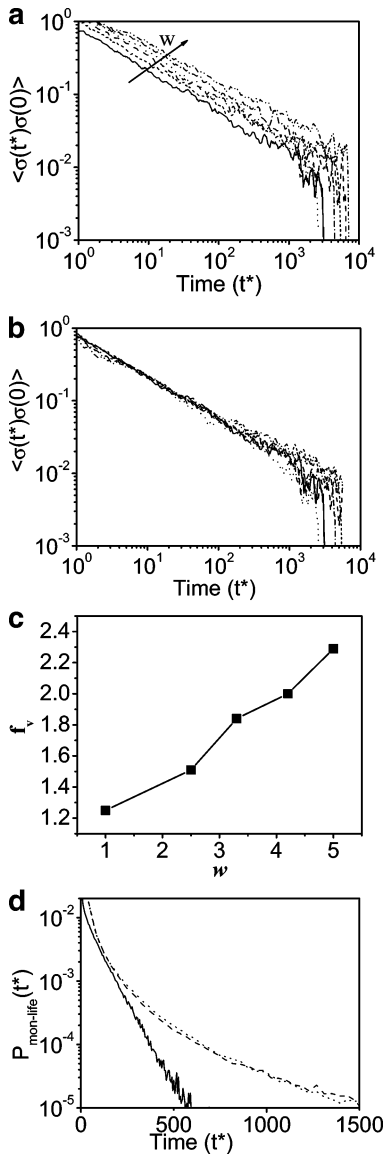

Figure 5. (a) Stress ACF of filled systems with smooth particles, at a loading of $\phi = 0.089$ and at varying levels of attraction. w: 1.0 (short dash), 2.5 (dash), 3.3 (short dot), 4.2 (dash dot), 5.0 (dash dot dot); neat $N = 80$ (solid), $R_c = 2.5$. (b) Stress ACF of systems plotted in (a), replotted as superposed on the neat melt by vertical shifting, for different values of w: 1.0 (short dash), 2.5 (dash), 3.3 (short dot), 4.2 (dash dot), 5.0 (dash dot dot); neat $N = 80$ (solid). (c) Vertical shift factors used to superpose data shown in (a) onto neat data as a function of w (polymer−particle well depth). (d) Distribution of lifetimes of monomers in the first shell around the particle, for different particle descriptions and different values of LJ cutoff: smooth particle, $w = 3.3$, $R_c = 2.5$ (solid); rough particle, $w = 2.8$, $R_c = 2.5$ (dash); rough particle, $w = 2.6$, $R_c = 1.5$ (dot).

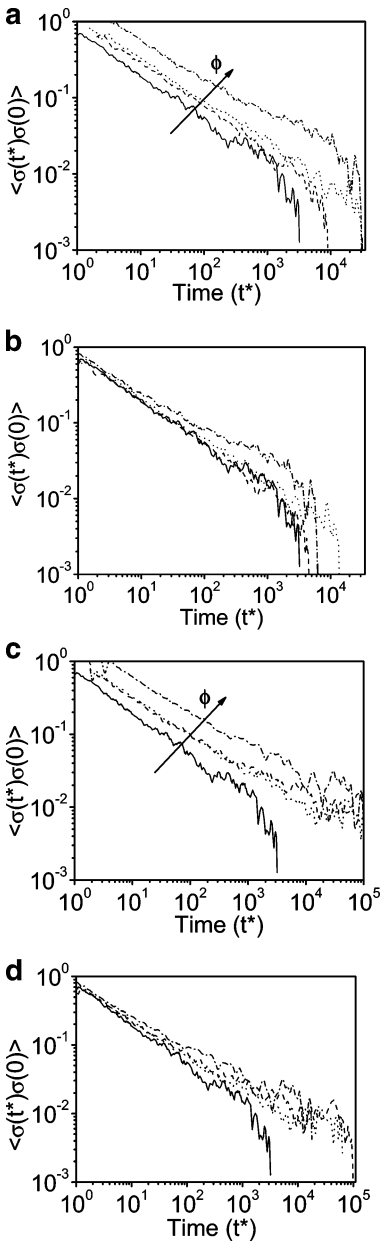

Figure 6. (a) Stress ACF of systems at varying particle loading, using rough particles, with LJ well depth, $w = 2.6$, and cutoff of 1.5: $\phi = 0.033$ (dash), $\phi = 0.045$ (dot), $\phi = 0.089$ (dash dot), neat $N = 80$ (solid). (b) Data from (a) horizontally shifted to superpose on the neat melt curve: $\phi = 0.033$ (dash), $\phi = 0.045$ (dot), $\phi = 0.089$ (dash dot), neat $N = 80$ (solid). (c) Stress ACF of systems at varying particle loading, using rough particles, with LJ well depth, $w = 5.1$, and cutoff of 1.5, $\phi = 0.033$ (dash), $\phi = 0.045$ (dot), $\phi = 0.089$ (dash dot), neat $N = 80$ (solid). These systems show an extended plateau beyond the terminal region of the neat melt. (d) Data from (c) horizontally shifted to superpose onto the neat melt curve: $\phi = 0.033$ (dash), $\phi = 0.045$ (dot), $\phi = 0.089$ (dash dot), neat $N = 80$ (solid).

renormalization of the absolute value of the stress autocorrelation. This result indicates a uniform upward shift in Rouse mode relaxation times. In fact, we find that the results for the filled systems can be superposed onto the neat melt curve by shifting along the vertical axis (Figure 5b,c). Alternatively, we can perform a shift along the time axis: we find that the two shift factors approximately follow the relationship $f_V \sim f_H^2$, where f_V and f_H are the vertical and horizontal shift factors, respectively. This is as expected from the Rouse model. At this loading of smooth particles, no deviation from Rouse-like behavior in the form of a plateau is seen, even for strong polymer−particle attractions.

We have also performed simulations with rough particles to determine whether the particle nature (smooth vs rough) plays a role in reinforcement. We find that for a long-range cutoff ($R_c = 2.5$) a similar shift in Rouse relaxation times occurs, but no deviation from Rouse behavior is observed. Similarly, for a short-range attraction with $w = 2.6$, we also see a uniform shift (Figure 6a,b). This shows that regardless of the particle nature at relatively high (∼9%) volume fraction all polymers are in the "interfacial zone" and felt the same effect of renormalized Rouse dynamics.

3.4.3. Reinforced Systems. With ∼9% volume fraction we fail to observe a reinforcing plateau regardless of the particle−polymer interactions. We therefore explored the effect of the volume fractions. First we consider the case of short chains (N

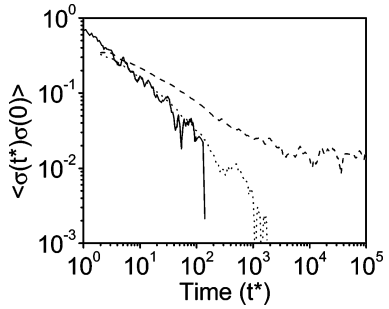

Figure 7. Stress ACF of filled systems with smooth particles and chains of length 20, plotted after vertical shifting to superpose the filled systems onto the neat melt data at short times, $\phi = 0.17$ (dot), $\phi = 0.25$ (dash), neat $N = 20$ (solid). At the highest volume fraction of 0.25 a plateau is seen, apparently due to jamming [shift factors: 8 ($\phi = 0.17$), 32 ($\phi = 0.25$)].

$= 20$) at higher loadings ($\varphi = 0.17$ and 0.25). In this system the particles are smooth, and the particle−polymer interactions are long-ranged with a strong attractive well ($R_c = 2.5$, $w = 5.0$). The stress ACF for both volume fractions is plotted in Figure 7. Both systems show an increase in the stress ACF for all times. A vertical shift was used to superpose the results for $\varphi = 0.17$ onto the neat melt curve. This indicates that the particles are causing a uniform increase in the Rouse mode relaxation times, just as in the previous results for long chains and smooth particles. However, the $\varphi = 0.25$ data cannot be readily superposed onto the neat melt data. In addition, the stress ACF does not decay within run times, indicating solidlike behavior. This is evidence for relaxation processes that differ significantly from those exhibited by a neat melt. We make the conjecture that this change in physics is primarily a consequence of "jamming" of the particles. It is known that, for well-dispersed spheres, the jamming due to percolation occurs at volume fractions higher than ~0.30.[46] For this level of particle−polymer attraction, each spherical particle has one or two layers of chain monomers closely associated with it. If we assume that there is only one monolayer associated with each particle, then the effective volume fraction is increased to $\varphi = 0.425$, which is clearly above the percolation threshold. This solidlike behavior also manifests itself in the MSD of the particles, showing essentially complete localization. This particle jamming reinforcement is consistent with the experimentally based conjectures of Wang et al.[13] and the simulations of Ganesan et al.[26]

In our search for particle−polymer network-based reinforcement we next considered the case of rough particles with short-range ($R_c = 1.5$) attractive polymer−particle interactions and chain length $N = 80$. The stress response of systems at three different particle loadings for strongly attractive ($w = 5.1$) interactions are plotted in Figure 6c,d. As volume fraction is decreased, the upward renormalization of Rouse relaxation times is less pronounced because a greater fraction of the matrix is in the bulk region. At long times, a prominent plateau is evident, indicating that there is a separation in both the spatial and time scales of the interfacial and bulk regions.

However, this effect is not as simple as it might first appear to be. In several of the runs with this set of parameters the reinforcement was observed at a much smaller level or, in some cases, not at all. This implies that nonequilibrium effects are at play.

3.4.4. Nonequilibrium Effects. The nonequilibrium reinforcement effects that we observe appear to be a consequence of long-lived structures, dependent on system preparation. To understand how this occurs, we must examine the system preparation in detail.

The strongly attractive rough particle systems were created in two different ways, which we will denote as method 1 and method 2. In both methods, four nanoparticles were placed at the fcc sites of a cubic simulation box. In method 1, described earlier, the polymer chains were placed in the box in a linear configuration, at low density. The system was then compressed using an NPT simulation to the proper melt density *without attractive interactions*. Once the appropriate density was reached and the chains had relaxed, the attractions were turned on. In contrast, in method 2 one-fourth of the chains were generated as self-avoiding random walks around one particle. This dilute configuration was then reproduced four times to create the total system. The system was compressed to the proper density, but in this case *attractive interactions were turned on from the beginning*.

If the systems were truly equilibrated, then, the final results would not depend on the starting state. However, we find that, on average, method 1 systems show plateaus in the stress ACF, while method 2 systems do not (Figure 8a). This provides direct evidence that the systems do not equilibrate, even after very long run times (in excess of 500 000). A comparison of the particle−particle radial distribution functions shows that the particle configuration is essentially the same for both methods (Figure 8b). This result implies that differences in network structure are responsible for the different relaxation behavior. To quantify this difference, we calculate the number of network structures, (i.e., bridges, loops, dangles, and trains) in static snapshots of the system and average them over the simulation runs. We also count the number of chains participating in these network structures. This is important because the far field nature of polymer immobilization by the particles is related to the fraction of chains that have segments adsorbed on the particle surfaces. These two quantities are plotted in Figure 8c,d. These results show that method 1 consistently has a higher number of structures as well as a higher number of chains involved in structures.

3.4.5. A Study of "Toy" Systems. The previously discussed simulations have shown that melt structure plays an essential role in reinforcement. However, we are unable to isolate the contribution from each type of structure in these systems, and we are also unable to determine whether there is a critical threshold of structure below which reinforcement does not occur. To improve our understanding of the role played by network structure, we have performed a set of simulations using telechelic chains, i.e., involving attractive interactions only between the chains ends and the "rough" particles. These attractions follow the same LJ potential used earlier, i.e., a cutoff of 1.5. Further, we randomly selected chains which can only form bridges between different particles, loops to the same particle, or are dangling chains with only one end attached to a surface. The fraction of chains that participate in these different network structures are varied in a series of simulations. We are thus able to systematically examine the role of these different network components in the reinforcement. A typical system has 30 chains of $N = 80$ and 4 filler particles. We have found that the particles agglomerate if just the chain ends are attracted to the particle surface, while the rest of the monomer−filler interactions are repulsive. To prevent this clustering, the remaining monomers are made weakly attractive to the fillers, using $w = 0.06$ with a cutoff of 1.5.

The stress autocorrelation function is plotted in Figure 9a. Reinforcement is observed in all cases, but the presence of dangles alone does not yield a plateau in the stress modulus. Loops can lead to a plateau, suggesting that they can form

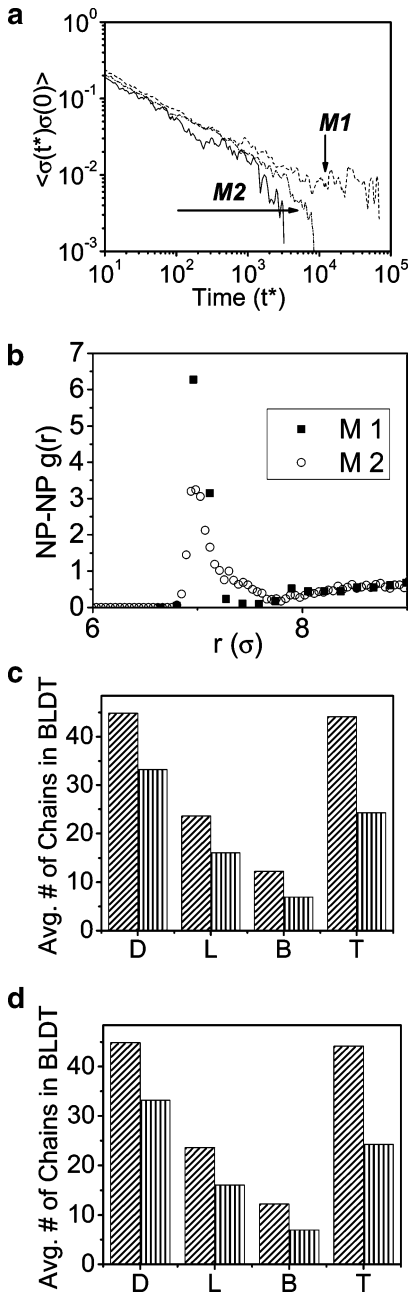

Figure 8. (a) Stress ACF compared for systems prepared by method 1 (M1) and method 2 (M2): M1 (dash), M2 (dot), neat $N = 80$ (solid). System is $\phi = 0.045$ and $w = 5.1$, with $R_c = 1.5$. (b) Particle−particle radial distribution function: M1 (filled squares), M2 (open circles). (c) Average number of network structures (dangles, loops, bridges, and trains, D, L, B, and T): M1 (inclined stripes), M2 (vertical stripes). (d) Average number of chains involved in network structures: M1 (inclined stripes), M2 (vertical stripes).

trapped "entanglements" presumably if long enough. Short loops are expected to act more like brushes and give no reinforcement.[47] The bridge systems display the most prominent plateau.

In order to see how the number of free chains in the system affects the stress response, we took the bridges-only structure and cut a number of chains in half: these cut chains thus only form dangles. We analyzed systems with 12 and 24 cut chains. The stress autocorrelation function is plotted in Figure 9b; the reinforcement of the systems drops with increasing number of free chains in the system. There is no reinforcement in the system with just 6 bridges. We thus conclude that both bridges and loops can provide reinforcement, with the bridges giving

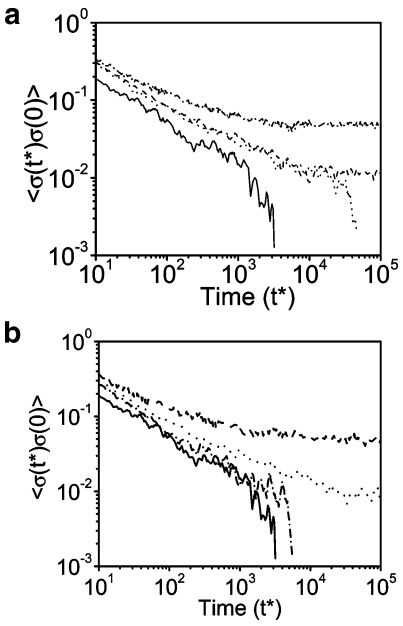

Figure 9. (a) Stress ACF of telechelic systems, compared for different structures: dangles (dot), loops (dash), bridges (dash dot), and neat $N = 80$ (solid). Particle−chain end interaction: $w = 5.1$, $R_c = 1.5$, and $\phi = 0.089$. (b) Stress ACF of telechelic system with bridges only and varying number of free chains: 0 free chains (dash), 12 free chains (dot), 24 free chains (dash dot), and neat $N = 80$ (solid). Particle−chain end interaction $w = 5.1$, $R_c = 1.5$, and $\phi = 0.089$.

rise to more solidification than the loops. However, a minimum number must exist for reinforcement.

3.5. Discussion. It is readily apparent that both a transient polymer network and also particle agglomeration can play important roles in yielding the reinforcement behavior that is of interest. Several of our results point to the fact that the specifics of the system considered play a role in determining the relative importance of these two effects.

First, we focus on the role of the interaction between the polymer and particles. As we have stressed, two criteria must be met before a particle−polymer transient network can lead to reinforcement: (i) the interactions must be short-ranged so that the interfacial zone occupies significantly less volume than the bulk region, and (ii) the particle−polymer interactions must be strong enough that parts of the polymer chains are essentially immobilized for long periods of time compared to the observation time. Once these two conditions are satisfied, the interfacial and bulk regions will be both spatially and temporally distinct, and we will observe two characteristic relaxation times. If a melt structure is present that couples the locally adsorbed monomer dynamics to longer-scale chain dynamics, then network-like polymer-driven reinforcement is observed. Systems that do not satisfy these two requirements can only show a uniform shift in relaxation times or yield reinforcement that is dominated by particle agglomeration. If the interactions are not strong enough, then the interfacial polymer can desorb and be replaced by bulk polymer. In both of these cases all of the polymer chains sample both regions during the course of the simulations, and a uniform shift in relaxation times is observed. The relaxation spectrum is also uniformly shifted in the case of long-range interactions where the bulk polymer is slowed at the same rate as the interfacial polymer. These results, of course, point strongly to the importance of system specifics. Namely, the type of polymer−particle interactions and the particle volume fraction determine the mechanical properties of the nanocomposites. Perhaps, even more saliently, they stress the crucial role of processing, especially since systems that are

significantly reinforcing are essentially glasslike in their response.[48] While we have made no attempt to extend our simulation methods to assist the equilibration of these systems, e.g., through the use of parallel tempering methods,[49] they essentially point to the fact that the initial state of the polymer network determines the mechanical reinforcement observed. Similarly, we expect that the initial state of particle agglomeration must also play a corresponding role.

Finally, it is important to understand the role of percolation in this context.[10] All of our simulations are conducted on such small systems that we are only modeling spaces which are ~10 nm on a side. We have observed the formation of either a spanning polymer or particle network in these cases, which we have identified as being associated with percolation. Wang et al.[13] correctly point out that it is unnecessary for a percolating structure to exist to obtain reinforcement: rather, a large aggregate of either the particles or the polymer is sufficient to yield long-lived reinforcement. We echo this same concept but stress that our simulations are incapable of distinguishing between these two scenarios (i.e., between large aggregates or percolating clusters).

4. Conclusions

We have performed an extensive study of the factors controlling the reinforcement afforded when nanoparticles are added to amorphous polymer matrices. Our results show that, first of all, the attraction between the particles and the polymer has to be strong enough to allow for the particles to be uniformly dispersed in the polymer matrix. Further, for rough particles with strong, short-ranged polymer−particle interactions, we find that a local layer of monomers surrounding a particle are immobilized but that the rest of the matrix is still mobile. This apparently contradictory set of requirements then allows the material to behave as a soft solid driven by the formation of a transient polymer−particle network. If the interactions were too long ranged, then, the polymer matrix becomes glassy and reinforcement in these cases is closer in spirit to the jamming that has been observed in a range of other systems: this effect does not possess any polymer-like character. In all of these cases, the reinforcement is only achieved in cases where the monomers on the particle surface are strongly immobilized: we thus show that the behavior of these systems is strongly dominated by nonequilibrium effects, which further complicate the interpretation of both experiments and simulations.

We end by stressing that the mechanical reinforcement observed in experimental systems can be a consequence of either particle agglomeration or a polymer-based network. However, neither of these two effects is universally dominant, and the relative contribution of each depends strongly on the particle−polymer interaction energy and range, the particle volume fraction, and quite possibly the state of particle dispersion. We are currently investigating the effects of particle agglomeration on stress reinforcement, but initial results point to particle immobilization as playing a central role in conjunction with agglomeration.

Acknowledgment. The authors thank the National Science Foundation (NIRT CMS-0404291, MSERC CMS-0310596, NSEC for Directed Assembly of Nanostructures DMR-0117792, and SKK DMR-0413755 grant) for funding of this research. We also thank Prof. Venkat Ganesan for discussing his results with us prior to their publication and Prof. Shi-Qing Wang and Prof. Sandy Sternstein for sharing their viewpoints on the source of reinforcement. We also thank Josh Hurst for his help in proofreading this manuscript.

Nomenclature

LJ monomer diameter (length scale): $\sigma = \sigma_{\text{polymer}} = 1$
LJ potential well depth (energy scale): $\epsilon = \epsilon_{\text{polymer}} = 1$
reduced time: $t^* = \sqrt{\epsilon/(m\sigma^2)}t$
reduced temperature: $T^* = k_B T/\epsilon$
reduced density: $\rho^* = 0.85 = \rho\sigma^3$
reduced viscosity: $\eta^* = \eta\sigma^3/\epsilon$
reduced stress correlation: $\sigma^*_{\alpha b} = \sigma_{xy}(\sigma^3/\epsilon)$

References and Notes

(1) Manias, E.; Huh, J. Y.; Wang, Z. M.; Wu, L.; Kuppa, V. In *Multifunctional Polymer/Inorganic Nanocomposites,* 5th ICIM; Smart Systems and Nanotechnology, 2003.
(2) Krishnamoorti, R.; Vaia, R. A. In *Polymer Nanocomposites: Synthesis, Characterization, and Modeling*; ACS Symposium Series; American Chemical Society: Washington, DC, 2002.
(3) Nielsen, L. E.; Landel, R. F. *Mechanical Properties of Polymers and Composites;* Marcel Dekker: New York, 1994.
(4) Havet, G.; Isayev, A. I. *Rheol. Acta.* **2003**, *42*, 47−55.
(5) Sternstein, S. S.; Ramorino, G.; Jiang, B.; Zhu, A. J. *Rubber Chem. Technol.* **2005**, *78*, 258−270.
(6) Zhang, Q.; Archer, L. A. *Langmuir* **2002**, *18*, 10435−10442.
(7) Krishnamoorti, R.; Vaia, R. A.; Giannelis, E. P. *Chem. Mater.* **1996**, *8*, 1728−1734.
(8) Hsieh, A. J.; Moy, P.; Beyer, F. L.; Madison, P.; Napadensky, E.; Ren, J. X.; Krishnamoorti, R. *Polym. Eng. Sci.* **2004**, *44*, 825−837.
(9) Xu, L.; Reeder, S.; Thopasridharan, M.; Ren, J. X.; Shipp, D. A.; Krishnamoorti, R. *Nanotechnology* **2005**, *16*, S514−S521.
(10) Krishnamoorti, R.; Ren, J. X.; Silva, A. S. *J. Chem. Phys.* **2001**, *114*, 4968−4973.
(11) Zhu, A. J.; Sternstein, S. S. *Compos. Sci. Technol.* **2003**, *63*, 1113−1126.
(12) Sternstein, S. S.; Zhu, A. J. *Macromolecules* **2002**, *35*, 7262−7273.
(13) Zhu, Z. Y.; Thompson, T.; Wang, S. Q.; von Meerwall, E. D.; Halasa, A. *Macromolecules* **2005**, *38*, 8816−8824.
(14) Gersappe, D. *Phys. Rev. Lett.* **2002**, *89* (5), Art. No. 058301.
(15) Salaniwal, S.; Kumar, S. K.; Douglas, J. F. *Phys. Rev. Lett.* **2002**, *89* (25) Art. No. 258301.
(16) Vacatello, M. *Macromolecules* **2001**, *34*, 1946−1952.
(17) Vacatello, M. *Macromolecules* **2003**, *36*, 3411−3416.
(18) Vacatello, M. *Macromol. Theory Simul.* **2003**, *12*, 86−91.
(19) Vacatello, M. *Macromolecules* **2002**, *35*, 8191−8193.
(20) Desai, T.; Keblinski, P.; Kumar, S. K. *J. Chem. Phys.* **2005**, *122* (13), Art. No. 134910.
(21) Ozmusul, M. S.; Picu, C. R.; Sternstein, S. S.; Kumar, S. K. *Macromolecules* **2005**, *38*, 4495−4500.
(22) Starr, F. W.; Schroder, T. B.; Glotzer, S. C. *Phys. Rev. E* **2001**, *64* (2), Art. No. 021802.
(23) Starr, F. W.; Schroder, T. B.; Glotzer, S. C. *Macromolecules* **2002**, *35*, 4481−4492.
(24) Starr, F. W.; Douglas, J. F.; Glotzer, S. C. *J. Chem. Phys.* **2003**, *119*, 1777−1788.
(25) Hooper, J. B.; Schweizer, K. S. *Macromolecules* **2005**, *38*, 8858−8869.
(26) Pryamitsyn, V.; Ganesan, V. *Macromolecules* **2006**, *39*, 844−856.
(27) Borodin, O.; Bedrov, D.; Smith, G. D.; Nairn, J.; Bardenhagen, S. *J. Polym. Sci., Part B: Polym. Phys.* **2005**, *43*, 1005−1013.
(28) Smith, G. D.; Bedrov, D.; Li, L. W.; Byutner, O. *J. Chem. Phys.* **2002**, *117*, 9478−9489.
(29) Kremer, K.; Grest, G. S. *J. Chem. Phys.* **1990**, *92*, 5057−5086.
(30) Stoddard, S. D.; Ford, J. *Phys. Rev. A* **1973**, *8*, 1504−1512.
(31) Allen, M. P.; Tildesley, D. J. *Computer Simulation of Liquids;* Oxford University Press: Oxford, 1987.
(32) Sen, S.; Kumar, S. K.; Keblinski, P. *Macromolecules* **2005**, *38*, 650−653.
(33) Humphrey, W.; Dalke, A.; Schulten, K. *J. Mol. Graphics* **1996**, *14*, 33−38.
(34) Starr, F. W.; Schroeder, T. B.; Glotzer, S. C. *Abstr. Pap. Am. Chem. Soc.* **2000**, *220*, U237−U237.
(35) Wallace, M. L.; Joos, B.; Plischke, M. *Phys. Rev. E* **2004**, *70* (4), Art. No. 041501.
(36) Doi, M.; Edwards, S. F. *The Theory of Polymer Dynamics;* Clarendon: Oxford, 1986.
(37) Vladkov, M.; Barrat, J.-L. *Macromol. Theory Simul.* **2006**, *15* (3), 252−262.
(38) Nakatani, A. I.; Chen, W.; Schmidt, R. G.; Gordon, G. V.; Han, C. C. *Polymer* **2001**, *42*, 3713−3722.
(39) Botti, A.; Pyckhout-Hintzen, W.; Richter, D.; Straube, E.; Urban, V.; Kohlbrecher, J. *Physica B* **2000**, *276*, 371−372.
(40) Asakura, S.; Oosawa, F. *J. Chem. Phys.* **1954**, *22*, 1255−1256.

(41) Koshy, R.; Desai, T.; Keblinski, P.; Hooper, J.; Schweizer, K. S. *J. Chem. Phys.* **2003**, *119*, 7599−7603.
(42) Mackay, M. E.; Dao, T. T.; Tuteja, A.; Ho, D. L.; Van Horn, B.; Kim, H. C.; Hawker, C. J. *Nat. Mater.* **2003**, *2*, 762−766.
(43) Kairn, T.; Daivis, P. J.; Ivanov, I.; Bhattacharya, S. N. *J. Chem. Phys.* **2005**, *123* (19), Art. No. 194905.
(44) Ganesan, V.; Pryamitsyn, V.; Surve, M.; Narayanan, B. *J. Chem. Phys.* **2006**, *124* (22), Art. No. 221102.
(45) Leibler, L.; Rubinstein, M.; Colby, R. H. *Macromolecules* **1991**, *24*, 4701−4707.
(46) Stauffer, D.; Aharony, A. *Introduction to Percolation Theory;* Taylor & Francis: London, 1992.
(47) Milner, S. T.; Witten, T. A. *Macromolecules* **1992**, *25*, 5495−5503.
(48) Ren, J. X.; Krishnamoorti, R. *Macromolecules* **2003**, *36*, 4443−4451.
(49) Ayyagari, C.; Bedrov, D.; Smith, G. D. *J. Chem. Phys.* **2005**, *123* (12), Art. No. 124912.

MA070512Z